ORIGINAL PAPER

Millennial timescale resolution of rhyolite magma recharge at Tarawera volcano: insights from quartz chemistry and melt inclusions

Phil Shane · Victoria C. Smith · Ian Nairn

Abstract Most rhyolite eruption episodes of Tarawera volcano have emitted several physiochemically distinct magma batches ($\sim$1–10 km^3). These episodes were separated on a millennial timescale. The magma batches were relatively homogeneous in temperature and composition at pumice scale (>4 cm), but experienced isolated crystallisation histories. At the sub-cm scale, matrix glasses have trace element compositions (Sr, Ba, Rb) that vary by factors up to 2.5, indicating incomplete mixing of separate melts. Some quartz-hosted melt inclusions are depleted in compatible trace elements (Sr, Ti, Ba) compared to enclosing matrix glasses. This could reflect re-melting of felsic crystals deeper in the crystal pile. Individual quartz crystals display a variety of cathodoluminescence brightness and Ti zoning patterns including rapid changes in melt chemistry and/or temperature ($\sim$50–100°C), and point to multi-cycle crystallisation histories. The Tarawera magma system consisted of a crystal-rich mass containing waxing and waning melt pockets that were periodically recharged by silicic melts driven by basaltic intrusion.

Keywords Rhyolite · Okataina · Recharge · Quartz · Melt inclusions · Magma

Communicated by T.L. Grove.

P. Shane (✉)
School of Geography, Geology and Environmental Science,
University of Auckland, Private Bag 92019, Auckland 1142,
New Zealand
e-mail: pa.shane@auckland.ac.nz

V. C. Smith
Department of Earth Sciences, University of Bristol,
Bristol BS8 1RJ, UK

I. Nairn
45 Summit Rd, RD 5, Rotorua, New Zealand

I. Nairn
GNS Science, Wairakei Research Centre, Taupo, New Zealand

Introduction

Models of the formation and rejuvenation of large scale ($\geq$10^3 km^3) rhyolite magma bodies highlight the role of mafic intrusion at depth, leading to prolonged accumulation, re-melting of plutonic fore-runners and silicic recharge (Bachmann et al. 2002; Hildreth and Wilson 2007; Lipman 2007; Wark et al. 2007). Similar processes have been proposed for the growth of silicic plutons (e.g., Wiebe et al. 2004, 2007). Textural, geochemical, isotopic and field studies of both plutonic and volcanic rocks point to incremental growth of their parent magma bodies (e.g., Glazner et al. 2004). Geophysical studies have failed to detect large bodies of mobile magma (more than $\sim$50% melt) in the present-day crust, but have revealed zones of partial melt (<30% melt) beneath volcanoes (see Bachmann et al. 2007). Thus, the eruption of crystal-poor rhyolites is thought to represent extraction of interstitial silicic melt from crystal-rich mush zones (e.g. Hildreth 2004; Bachmann and Bergantz 2004); while the eruption of voluminous unzoned crystal-rich dacitic ignimbrites may represent the more complete remobilisation of the mush zone or cooling pluton (e.g., Bachmann et al. 2002, 2007).

Further insights into the dynamics of the growth of silicic magma bodies can come from tectonically rifted

regions with thin crust, where high rhyolite magma production and leakage rates have led to frequent eruptions. This study focuses on Tarawera volcano in the Taupo Volcanic Zone (TVZ), North Island, New Zealand. Tarawera was built during four rhyolite eruption episodes over the last 22 kyears of intracaldera activity at the Okataina Volcanic Centre (OVC) (Nairn 2002) (Fig. 1). Each episode released 5–10 km^3 of rhyolite magma, with subordinate basalt injection, separated by repose periods of >1,000 years.

Our previous studies of individual Tarawera rhyolite eruption episodes have demonstrated the co-eruption of physiochemically discrete magma batches (Nairn et al. 2004; Shane et al. 2007, 2008). These studies generated pumice-clast-scale (>4 cm) mineralogical, chemical and intensive parameter data. Here we report a new dimension of sub-cm scale magmatic heterogeneity based on quartz chemistry and thermometry, and trace element chemistry of quartz-hosted melt inclusions and matrix glass within individual pumice clasts. The data record thermal and chemical signals from incremental rhyolite magma accumulation processes lasting <10^3 year.

Tectonic setting

The TVZ is the actively rifting on-land continuation of the Tonga–Kermadec arc, formed at the convergent plate boundary between the westerly subducted Pacific Plate and the partly continental Australian plate. Mesozoic greywackes outcrop east and west of the TVZ and probably underlie volcanic fill within the TVZ, either as tectonically stretched crust, or as rifted blocks separated by intrusive rocks (Stern et al. 2006). Heat flux from the TVZ is exceptionally high, 26 MW/km along strike (Stern et al. 2006), and similar to that of mantle-upwelling "hot spots" such as Iceland and Yellowstone. The high heat flux causes the brittle-to-ductile transition to occur at a shallow depth (typically 6–7 km) (Bryan et al. 1999). A seismic refraction profile across central TVZ has been modelled as quartzo-feldspathic upper crust down to 16 km (Stratford and Stern 2004). The depth interval ∼16–35 km has been interpreted as either mantle with extraordinarily low P wave velocity (6.9–7.3 km/s) containing significant melt bodies (Stratford and Stern 2004), or highly intruded mafic crust with 2% melt (Harrison and White 2004).

Fig. 1 Map of OVC showing the outline of Haroharo Caldera (∼50 ka), the location of post-25 ka rhyolite vents and deposits, and faults. *Inset*: map of North Island showing the location of TVZ
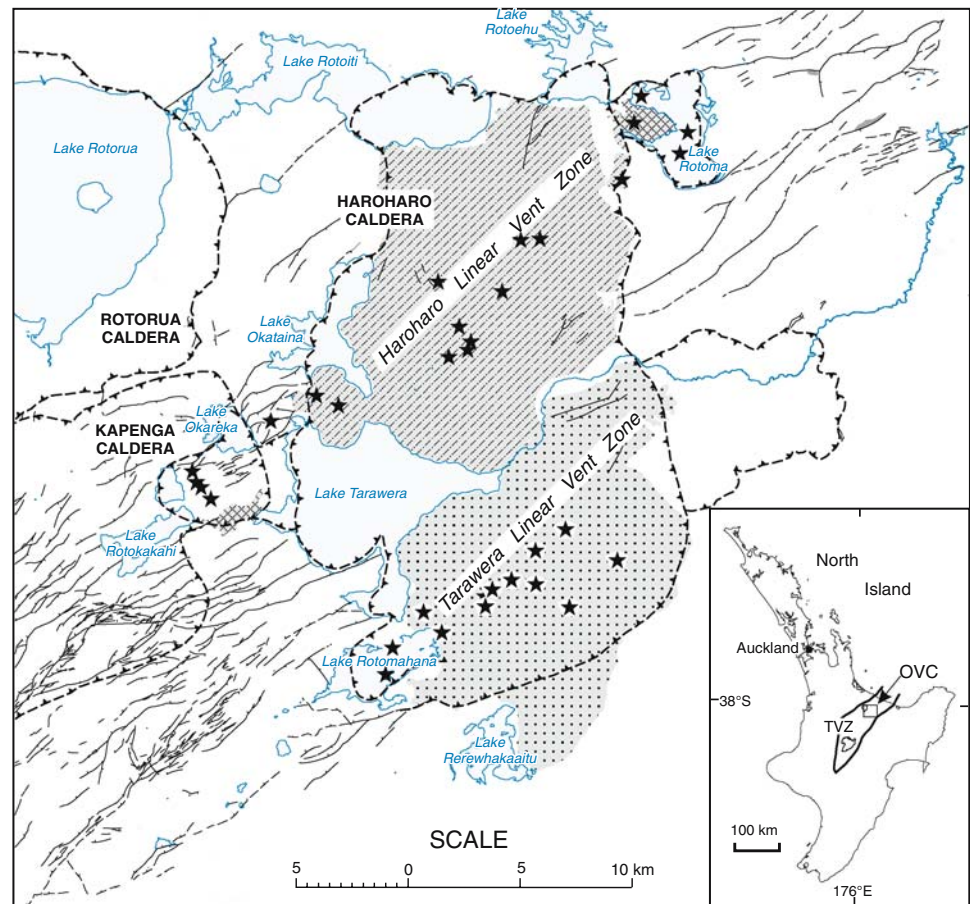
The eruption of voluminous (>100 km^3) rhyolite ignimbrites (~280 and ~50 ka) during caldera-forming episodes at OVC (Nairn 2002) demonstrates that large bodies of eruptible magma have previously accumulated beneath this area. The frequency and magnitude of eruptions at OVC has not been uniform over time (Nairn 2002; Smith et al. 2005), and thus the presence and size of magma bodies in the upper crust may have also varied greatly through time. Regions of low S wave velocity about 10–20 km wide at depths of ~6–11 km to south of the OVC could represent present-day zones of partial melt (Bannister et al. 2004). The resolution of the seismic data is low, but is consistent with magnetotelluric data that suggests the existence of conductive zones representing connected melts at depths of ~10 km (Heise et al. 2007).

Tarawera volcanism

Rhyolite eruption episodes

The OVC has been the site of numerous rhyolitic eruption episodes involving 1 to >100 km^3 of magma over the last >350 kyears (Nairn 2002), with much of its present morphology resulting from the >100 km^3 Matahina and Rotoiti caldera-forming ignimbrite eruptions at ~280 and 50 ka, respectively. The Tarawera massif consists of rhyolite lava domes and flows, with intercalated proximal pyroclastic flow and fall deposits, erupted during the last 22 kyears from vents in the southeast part of the OVC caldera. About 30 km^3 of magma has been erupted (Table 1) during four

major rhyolite episodes occurring at 21.8, 17.6, 13.6 and 0.7 ka (Table 1). The only historic eruption is a basaltic plinian fissure eruption in AD1886 (Nairn and Cole 1981). Multiple vents were involved in each eruption episode at Tarawera, and together define a broad SW–NE trending zone (Fig. 1). Each rhyolite episode produced pyroclastic falls and flows from plinian-style activity, and lava dome extrusion (Nairn et al. 2001; Nairn 2002; Speed et al. 2002; Darragh et al. 2006). There are no paleosols or significant hiatuses within deposits of any of the four rhyolite episodes, suggesting that episode durations were <100 years. Minimum episode durations of ~5–10 years have been estimated from the rates of silicic dome extrusion observed elsewhere (Nairn et al. 2001). There is no consistent relationship between duration of quiescence and volume of the subsequent episode (Table 1).

The role of basalt at Tarawera

Some evidence for the involvement of basaltic magma is found in every Tarawera eruption episode. The 21.8 ka episode started with the sub-plinian eruption of basaltic scoria, and basalt-rhyolite hybrid and mingled pumices occur in the initial rhyolite fall deposits (Shane et al. 2008). The 17.6 ka eruptives include some rhyolite pumices that contain andesitic to rhyodacitic hybrid glass blebs ≤1 cm in size, accompanied by xenocrystic olivine, calcic plagioclase and magnesian orthopyroxene phases typical of basaltic to andesitic magmas (Shane et al. 2007). No basalt component is found in the 13.6 ka deposits erupted from the main vent, but rare basaltic and andesitic clasts occur in

Table 1 Selected characteristics of magma batches in Tarawera eruption episodes

Magma	Mineralogy	Crystal (%)	SiO$_2$	Sr	Eu/Eu*	K$_2$O	T (°C)	fO$_2$	Vol (km^3)
0.7 ka (Kaharoa)									
T1[a]	Bio > Hb > Cgt ± Opx	2–25	77.5	52	0.44	4.26	–	–	2.0
T2[a]	Bio > Cgt > hb ± Opx	20–40	76.2	107	0.65	4.13	–	–	2.0
Granitoid	Bio ± Opx ± Hb	100	73.2	142	0.50	–	–	–	–
13.6 ka (Waiohau)	Opx + Hb	5–10	76.8	103	0.63	3.40	772	0.47	10.0
17.6 ka (Rerewhakaaitu)									
T1	Opx > Hb ± Cgt	<10	77.0	91	0.60	3.42	760	0.27	4.0
T2	Bio > Hb	>20	75.6	120	0.70	4.19	704	−0.45	1.5
T3	Opx + Hb	20	73.7	176	0.75	3.14	824	1.28	0.2
21.8 ka (Okareka)									
T1	Opx > Cgt > Hb ± Bio	9–18	77.0	77	0.47	3.81	754	0.24	0.3
T2[b]	Hb + Bio > Opx	–	–	–	–	4.16	724	−0.05	0.3
T3	Opx + Hb > Cgt ± Bio	24–34	75.3	126	0.68	3.43	794	0.82	4.5

SiO$_2$ (wt%) and Sr (ppm) = whole rock; K$_2$O (wt%) = glass; T and fO$_2$ (ΔNNO) from Fe–Ti oxides

Bio biotite, *Hb* hornblende, *Cgt* cummingtonite, *Opx* orthopyroxene

[a] No equilibrium Fe–Ti oxides

[b] Ash grade material only

a rhyolite breccia erupted during the episode from a satellite vent near Lake Rotomahana (Fig. 1) (Nairn 2002). The 0.7 ka rhyolite deposits contain a ubiquitous but subordinate population of basaltic and hybrid andesitic inclusions (Leonard et al. 2002; Nairn et al. 2004). The AD1886 event was entirely basaltic. Hydrothermal eruptions occurred close in time to the 17.6 and 0.7 ka episodes, from vents ∼20 km to NE and SW of Tarawera. The hydrothermal events suggest that intrusion of basalt occurred as laterally extensive dikes during these eruption episodes (Nairn 2002; Nairn et al. 2005).

Analytical techniques and data

Whole-rock XRF, matrix glass electron microprobe, and Fe–Ti oxide data for each Tarawera eruption episode have been previously published (Speed et al. 2002; Nairn et al. 2004; Shane et al. 2007, 2008). Here we summarize the earlier data and augment it with new REE, melt inclusion, and quartz data. The data is based on both pyroclastic pumice clasts and lava. However, melt inclusion data were obtained mostly from pumice fall deposits. All new data can be found in the Electronic Supplementary file. REE data were collected by laser ablation inductively coupled plasma mass spectrometry on fused glass beads at the Australian National University. Instrumentation includes a Lambda Physik Complex 110 ArF (193 nm) Excimer laser and a VG Fusions Plasmaquad PQ2 STE ICPMA spectrometer. Instrument calibration was via NIST 612 glass. Sample analyses were normalised to SiO_2 from XRF data obtained on the same samples. Detection limits of ∼5 ppb were obtained for all elements reported.

Trace elements in matrix glasses and melt inclusions (MIs) were determined by secondary ion mass spectrometry (SIMS) using a Caméca ims-4f instrument at the NERC facility, University of Edinburgh. A 6 nA primary ^{16}O-beam was used. The secondary ions were extracted at +4.5 keV energy, with a 75 eV offset, and 40 eV energy window. Samples were pre-sputtered for 2 min using a 50 μm beam. Secondary ions were collected for 10 cycles using a focussed 15 μm beam. The instrument was calibrated using NRM-610 (NIST) and M335 glass, BOG-1 Quartz, and Corderite-79528 standards. Uncertainties in element abundance are typically <5%. We also performed some reconnaissance analyses of quartz crystals to determine the abundance of a range of trace elements. The pre-sputter was 1 min and a 60 nA beam with a diameter of ∼15 μm was used. Analyses were background corrected and calibrated using quartz standards. The analysed quartz-hosted MIs lack signs of post-entrapment chemical alteration, including shrinkage bubbles, microlites, colored

glass and cooling-induced morphology changes (negative crystal shapes) (e.g., Skirius et al. 1990). Such features are generally less common in rapidly erupted plinian fall deposits such as those examined here.

Cathodoluminescence (CL) images of quartz crystals were collected using a Philips CL detector on a Philips XL30CP scanning electron microscope at the University of Edinburgh. The quartz crystals were analysed using a Cameca SX-100 electron microprobe at the University of Bristol. An accelerating voltage of 20 kV, current of 200 nA, and ∼15 μm beam were used. In order to get reliable Ti results at low abundance, Ti was analysed on four spectrometers simultaneously, three equipped with LPET crystals and the other with standard PET crystal, for 240 s. Al was simultaneously collected on a TAP crystal. Detection limits of ∼6 and 11 ppm, and errors of ±5 and ±10 ppm, were obtained for Ti and Al, respectively.

The Ti content in quartz (Ti_{qtz}) is related to temperature, following the TitaniQ equation: $T = -3765/[\log (Ti_{qtz}/X_{Ti}) - 5.69]$ (Wark and Watson 2006), where T = temperature in Kelvin and X_{Ti} = activity of Ti in the quartz. X_{Ti} was calculated by dividing the theoretical Ti present in rutile-saturated melt ($Ti_{rut-melt}$) by the Ti in the melt (matrix glass). $Ti_{rut-melt}$ (in ppm) was calculated using the equation of Hayden et al. (2005): $\log (Ti_{rut-melt}) = 7.95 - (5305/T) + (0.124 \times FM)$, where FM is a melt composition parameter calculated using the equation of Ryerson and Watson (1987).

Tarawera magmas

Rhyolite mineralogy and whole rock geochemistry

Each post-22 ka rhyolite eruption episode, except the 13.6 ka episode, involved two or three rhyolite magma types (Table 1). Broadly, all post-22 ka rhyolites can be discriminated by their ferromagnesian mineral assemblage and crystallinity. Biotite-bearing rhyolites are relatively crystal-rich (>20 vol.%) and have low Fe–Ti oxide equilibrium temperatures (700–750°C) (Table 1). Orthopyroxene-hornblende rhyolites are mostly crystal-poor (<20 vol.%) and have high Fe–Ti oxide equilibrium temperatures (760–820°C). The crystal populations in both crystal-rich and crystal-poor rhyolites are dominated by quartz and plagioclase, with cummingtonite sometimes occurring as a minor phase. Spinel, ilmenite, apatite and zircon (in deceasing abundance) are accessory phases.

All Tarawera rhyolites have high silica contents (73–77 wt%, anhydrous), but the whole rock composition does not relate to mineral assemblage or crystallinity in a simple manner. The biotite rhyolites and orthopyroxene-hornblende rhyolites overlap in composition (Table 1).

However, the former are distinguished by their high-K_2O matrix glasses (=melt) reflecting their higher degrees of crystallisation. The rhyolites emitted during each post-22 ka eruption episode occupy a narrow range in whole rock major element compositions (less than ∼4 wt% SiO_2; Fig. 2a), but some trace elements such as Sr display more variability (Fig. 2b). The widest compositional range is found in the 17.6 ka deposits (SiO_2 = 73–77.5 wt%; Sr = 80–179 ppm). The 13.6 ka deposits are the most homogeneous (SiO_2 = 76.4–77.8 wt%; Sr = 90–110 ppm). Across all post-22 ka deposits, the higher abundance major and trace elements, Al_2O_3, FeO (Fig. 2a), CaO, TiO_2, MgO, Sr, and Zr display negative correlations with SiO_2; while K_2O and Rb (Fig. 2c) show positive correlation. Na_2O, Ba, La, Ce, and Y show no significant correlation. These relationships are consistent with the fractionation of plagioclase, hornblende, pyroxene, Fe–Ti oxides and zircon. The rhyolites display negative Eu anomalies and high LREE/HREE ratios (Fig. 2e; Table 1) that also point to plagioclase, hornblende

and zircon fractionation. However, the lack of continuous linear trends on plots and lack of temporal relationships are not consistent with derivation of all Tarawera rhyolites from a common crystallising parent body. Moreover, there are no temporal trends in crystallinity, mineralogy, geochemistry, or T–fO_2 (Table 1; Fig. 2). However, all of the Tarawera rhyolites are part of the same T–fO_2 trend (Fig. 2d) suggesting similar source characteristics.

Granitoid lithics are found in the 0.7 ka pyroclastic deposits, but are absent in deposits of earlier episodes. Their low $\delta^{18}O$ value (3.03‰, Brown et al. 1998) reflects interaction with meteoric/hydrothermal fluids suggesting that the granitoids cooled at shallow depths. The granitoid lithics contain plagioclase, quartz, sanidine, biotite, rare resorbed orthopyroxene, Fe–Ti oxides, ±hornblende. They are characterised by relatively low SiO_2 (Fig. 2), reflecting their high crystallinity. Granitoid REE patterns are similar to those of rhyolites, but are the most enriched of the rocks examined (Fig. 2e).

Fig. 2 a–c Selected variation diagrams of the whole rock lava and pumice composition of Tarawera rhyolites (Speed et al. 2002; Nairn et al. 2004; Shane et al. 2007, 2008). Deposits are divided into their eruption episode (age) and magma type (T1-3) based on physiochemical characteristics (see legend in d). d T–fO_2 estimates for each magma type based on Fe–Ti oxide data (Shane et al. 2007, 2008; Shane new data). Note the 0.7 ka deposits lack Fe–Ti oxide equilibrium pairs. e Chondrite-normalised REE compositions of Tarawera rhyolites compared to granitoid lithics and basalt from the 0.7 ka episode (new data)
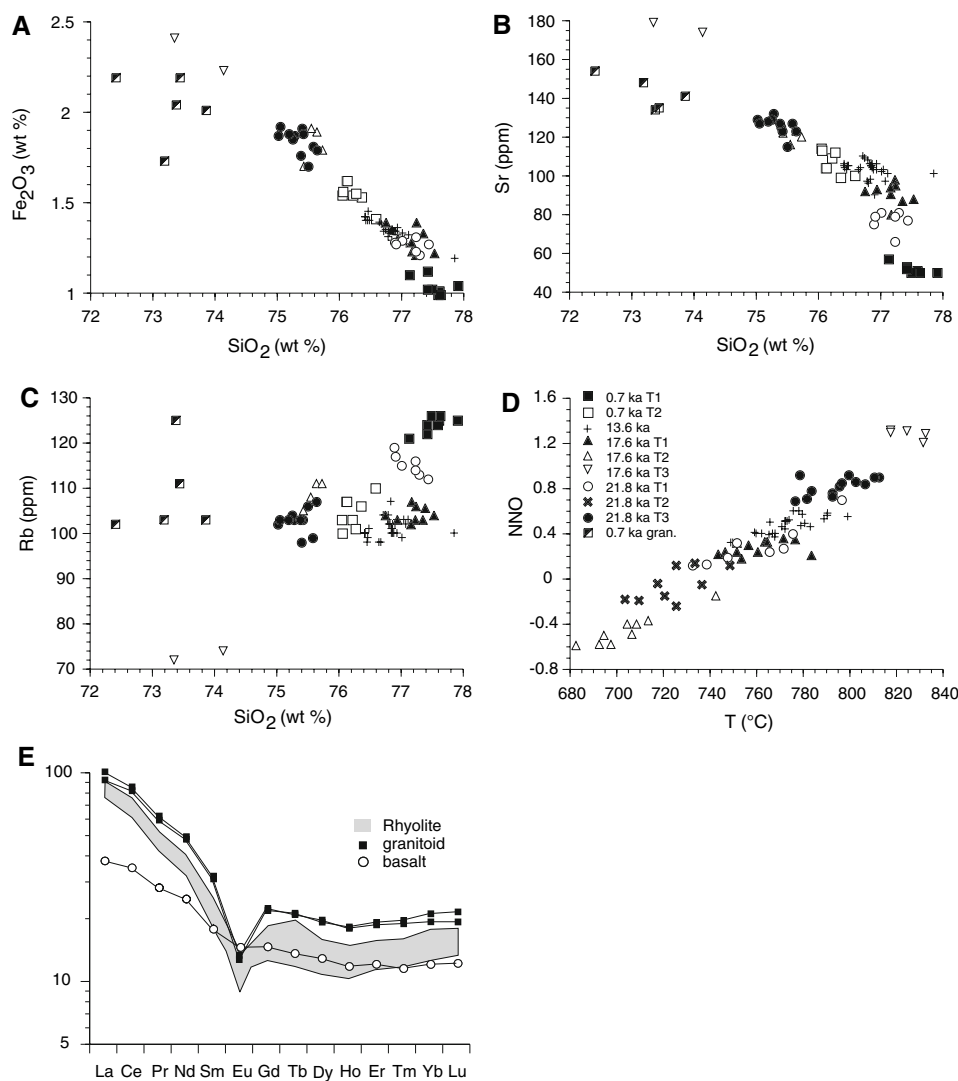
Magma batches

Multiple rhyolite magma batches were co-erupted during individual Tarawera episodes, and have been documented in detail in previous studies (Nairn et al. 2004; Shane et al. 2007, 2008). The magmas are defined as individual batches or types, on the basis of pumice, glass and mineral chemistry, T–fO_2, and mineral assemblage (Table 1; Fig. 3). Each magma batch is internally uniform in both chemical and physical parameters, especially major elements (SiO_2 varies by <1 wt%), but show some variations in whole-rock trace elements (Sr varies by <20 ppm; Zr <18 ppm; Rb <10 ppm). Analyses plot as clusters rather than linear arrays on variation diagrams (Figs. 2, 3). The ranges in matrix glass composition within a magma type are typically less than analytical error (e.g. K_2O ±0.3 wt%, CaO ±0.1 wt%) (Fig. 3). Similarly, ranges in Fe–Ti oxide equilibrium temperatures are narrow (<40°C), and the

crystal phases are compositionally distinct in each magma type (Fig. 3). In deposits of some episodes, the products of different rhyolite magmas are juxtaposed (i.e., as adjacent pyroclasts in a lapilli fall deposit, or as commingled glasses in pumices or lavas); in other cases an upward sequential change from one magma type to another is evident in the stratigraphic sequence.

Trace element modelling evidence has been advanced to discount simple fractional crystallisation links between the magma types within an eruption episode (Nairn et al. 2004). In addition, in the 17.6 ka episode, a less evolved but cooler magma type was erupted contemporaneously with a more evolved but hotter magma type, seemingly discounting simple parent–daughter relationships (Shane et al. 2007). Further, in both the 0.7 and 17.6 ka deposits, individual pumice clasts contain matrix glasses of two magmas (Fig. 3) showing that mingling of separate magma batches has occurred. In contrast, intermediate

Fig. 3 Examples of glass and crystal chemistry defining magma types in the Tarawera eruption deposits (Speed et al. 2002; Nairn et al. 2004; Shane et al. 2007, 2008; Shane new data). The magma types are also defined by other mineralogic and physiochemical parameters (Table 1). Mingled glass and crystal bimodal populations are examples of analyses from a single pumice clast in the deposit
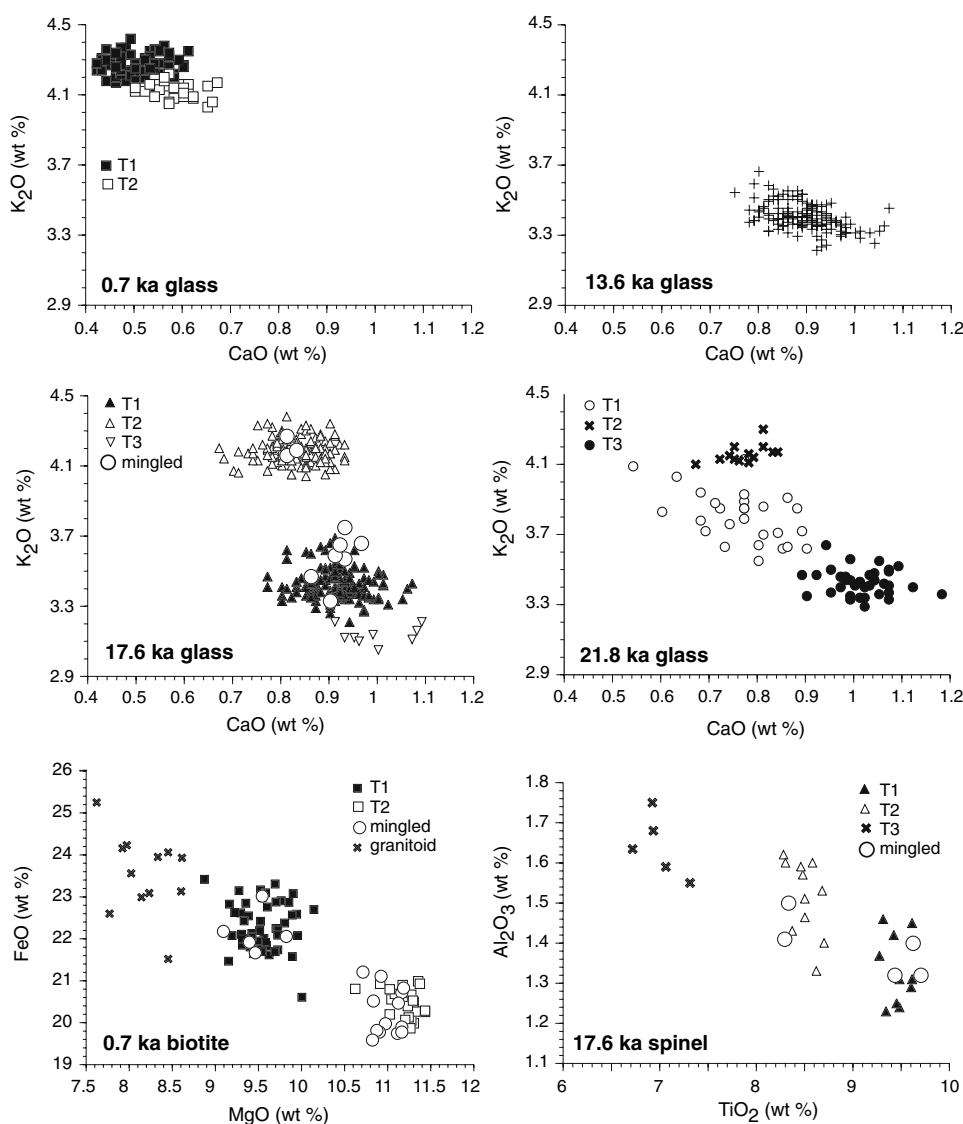
compositional glass, reflecting hybridisation of separate batches is rare. The mingled clasts also contain bimodal disequilibrium crystal populations (Fig. 3) and bimodal distributions in T–fO_2 estimates from Fe–Ti oxides (Shane et al. 2007, 2008). Fe–Ti oxides are known to be reset in weeks to months (Devine et al. 2003) and thus contact between the mingled magmas was short-lived and probably occurred in the conduit. These features point to separate pre-eruption accumulation and crystallisation histories for the co-erupted magma batches.

Trace element geochemistry of matrix glasses and quartz-hosted melt inclusions

The major element compositions of quartz-hosted MIs do not vary significantly from those of the accompanying matrix glasses, and appear relatively homogeneous (e.g., Nairn et al. 2004; Shane et al. 2007, 2008). However, trace element compositions of both MI and matrix glasses reveal more diversity within deposits from each of the Tarawera episodes, and within each of the magma batches. Contents of the more abundant trace elements (Sr, Rb, Zr, Ba and Ti) in matrix glasses can vary by a factor of up to ~ 2.5 within the defined magma batches. Such variations can occur within individual pumice clasts, while other clasts are relatively homogeneous based on multiple analyses (Fig. 4a, b). In quartz-hosted MIs, these elements also vary by similar factors within individual clasts (Fig. 4c–f). This suggests whole rock data reflect homogenisation of micro-variability in these deposits.

There are significant compositional differences between MIs and their accompanying matrix glasses in some deposits. In the 21.8 and 13.6 ka deposits, the MIs and matrix glasses have similar major element (SiO_2, Al_2O_3, Na_2O, K_2O) and minor trace element (Y, Nb, La, Ce) compositions. However, many of the MIs are depleted in Ti, Sr, and Ba by a factor of 0.3–0.5 relative to their accompanying matrix glasses (Fig. 4d, f). These differences indicate the quartz crystals could not have grown in the melt represented by the surrounding matrix glass; instead they must have crystallised in a more evolved magma.

In contrast, MIs from the 17.6 ka Tarawera event compositionally match their accompanying matrix glasses in the two magma types investigated (Fig. 4e). This suggests late-stage crystallisation had little influence on the melt composition, and the crystals grew in the melt in which they were erupted. Most MIs from the 0.7 ka event are enriched in Sr and Ti by a factor of 1.5–2 relative to their accompanying matrix glass (Fig. 4c). This MI enrichment, and accompanying depletion in Rb, follows a general trend expected from the crystallisation of 5–20% plagioclase (Fig. 4g), similar to the crystal contents found in these pumices.

Zoning in quartz

Quartz crystals in Tarawera deposits appear uniform when examined by optical microscopy and back-scattered electron imaging, but display zoning patterns when observed using cathodoluminescence (CL) techniques. The crystals show subtle internal oscillations in CL intensity (Fig. 5a, b), that resembles oscillatory zoning found in plagioclase, and is associated with diffusion and boundary layer effects (D'Lemos et al. 1997). In addition, some Tarawera quartz crystals display truncated patterns indicating periods of resorption and regrowth, similar to patterns observed in Bishop Tuff quartz (Peppard et al. 2001). Oscillatory and truncated patterns are particularly well developed in quartz of the 0.7 ka deposits (Fig. 5a), where large euhedral crystals are more common. Many of these crystals have bright cores with a gradation to darker rims.

Greater CL intensity contrasts and more irregular patterns occur within crystals of the 21.8 ka deposits (Fig. 5c–f). Some crystals display very bright mid-crystal zones or bands of variable width and irregular texture (Fig. 5e, f). Similar features have been recorded in quartz from granites (Wiebe et al. 2007). A few 21.8 ka crystals display bright rim mantles with sharp contacts (Fig. 5c). Eruption fragmentation in the 21.8 ka T2 and T3 ash deposits prevents full cross-section examination of many crystals.

Crystals from the 13.6 ka deposits are relatively subhedral to euhedral and all display similar CL patterns. They are characterised by bright rims, some of which are overgrowths surrounding truncated and corroded cores (Fig. 5b). Otherwise, they display fairly uniform CL patterns with no abrupt mid-crystal variations.

Quartz in granitoids from the 0.7 ka deposits are generally subhedral. They display complex networks of mostly randomly oriented dark lines (Fig. 6). These long, thin, and often irregular, lines run across most of the crystal, and smaller ones (10 µm-scale) feather-out from larger lines. These features are similar to those described by Bernet and Bassett (2005) as micro-cracks in plutonic quartz. We note that these "microcracks" are not observed in secondary electron or back-scattered electron images. The granitoid quartz also displays wide (up to ~ 500 µm) bands of differing CL intensity reflecting zoning (Fig. 6).

Composition of quartz and crystallisation temperatures

Previous workers have noted that the intensity of CL emissions within quartz crystals can be related to Ti content, and thus temperature (Wark and Watson 2006; Wark et al. 2007). Electron probe analyses of quartz in the 21.8, 13.6 ka and granitoids of the 0.7 ka deposits reveal a range in the most abundant trace elements Al (51–183 ppm and 4 outliers 190–300 ppm) and Ti (21–148 ppm). Their

Fig. 4 Multiple trace element analyses of matrix glass in different pumice clasts from the 0.7 ka (**a**) and 13.6 ka (**b**) deposits. Comparison of Ti and Sr contents in quartz MI (*open symbols*) and accompanying matrix glass (*filled symbols*) in Tarawera eruption deposits (**c–f**). For each eruption, samples are classified by their magma type (Table 1). **g** MI and matrix glass composition in 0.7 ka deposits plotted with a Rayleigh fractional crystallisation trend with tick marks at 5% plagioclase crystal extraction intervals
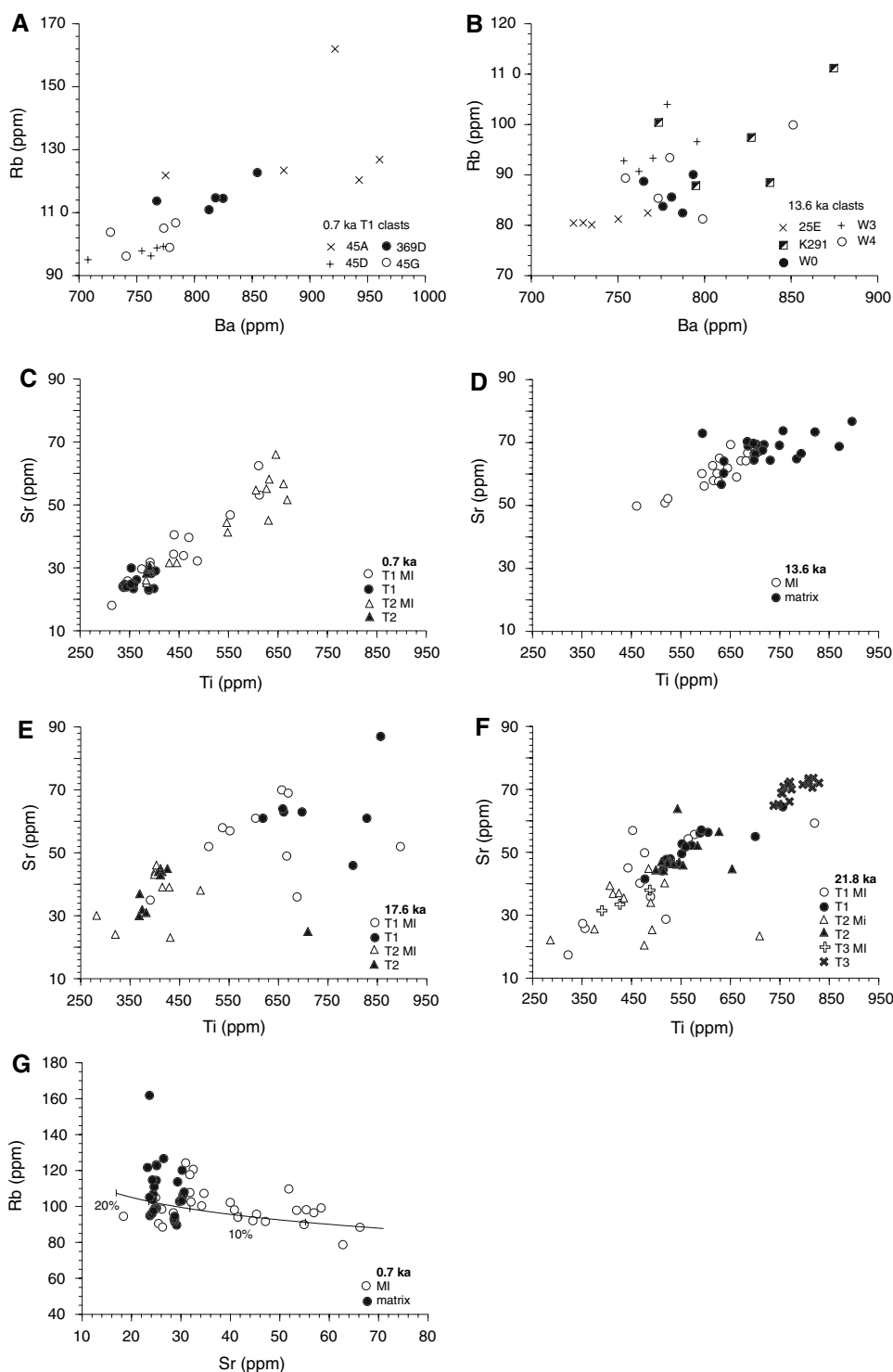
abundances display a positive linear relationship. The other elements determined by SIMS (Fe, Ca, Na, K, Li, Cl, F, Ge) each have concentrations <7 ppm. High Al and Ti contents correlate to high CL brightness in all crystals we examined. Thus, the CL intensity images are a proxy for Ti content and temperature variations during the crystal's growth history. Direct estimates of temperature were made

using TitaniQ based on Ti concentration in the quartz (see "Analytical techniques and data"). These estimates assume no significant change in the activity of Ti in the melt during the crystallisation history (see "Discussion").

We selected analytical locations and performed partial crystal traverses to investigate the irregular CL patterns in the 21.8 ka quartz population. Wide Ti variations were

Fig. 5 Examples of CL and Ti zoning in quartz. **a** 0.7 ka deposits (T1 magma). **b** 13.6 ka deposits. **c** 21.8 ka deposits (T2 magma). **d** 21.8 ka deposits (T3 magma). **e** 21.8 ka deposits (T2 magma). **f** 21.8 ka deposits (T3 magma)
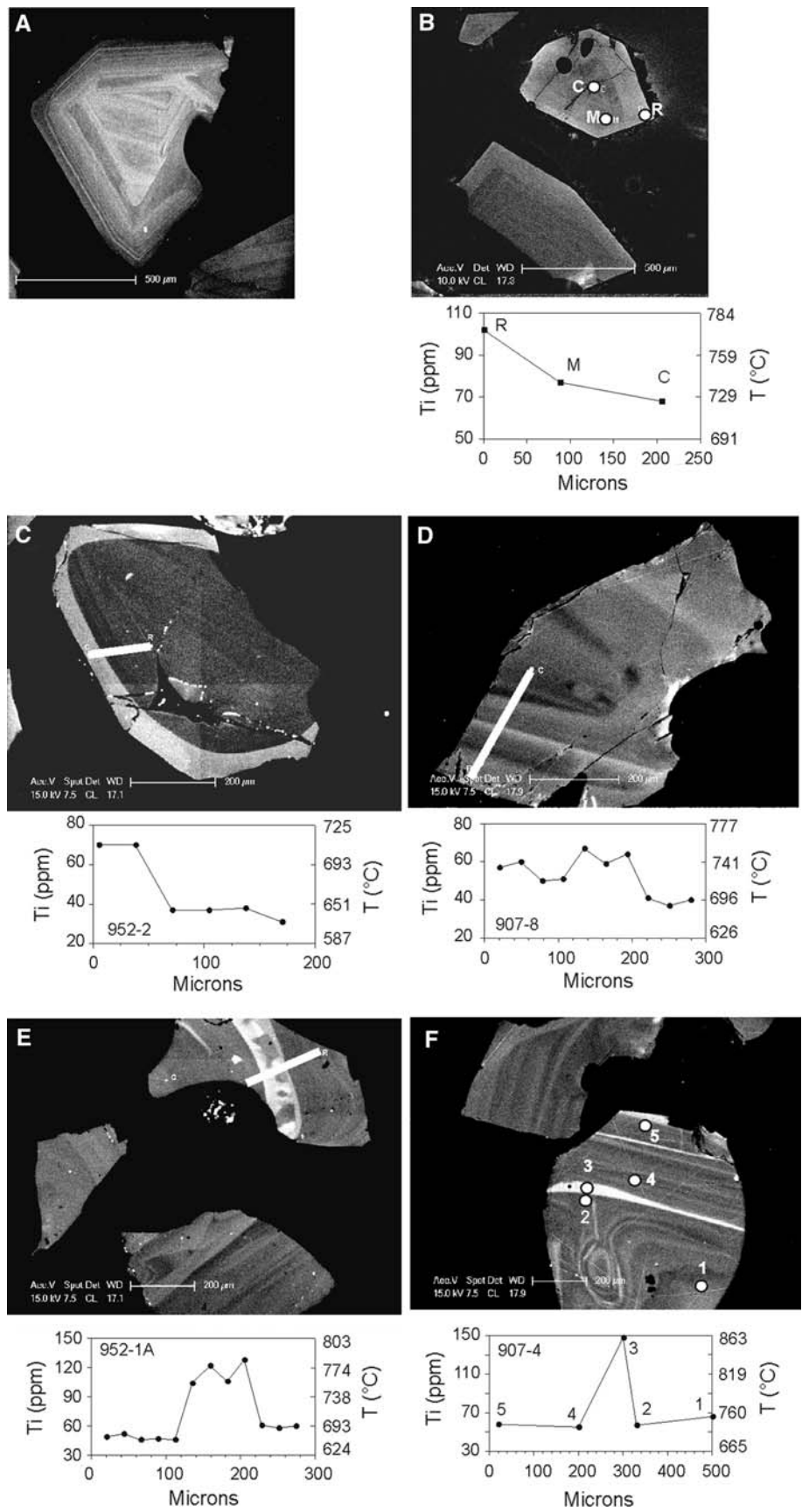
Fig. 6 Examples of CL and Ti zoning in quartz from granitoid clasts in the 0.7 ka deposits
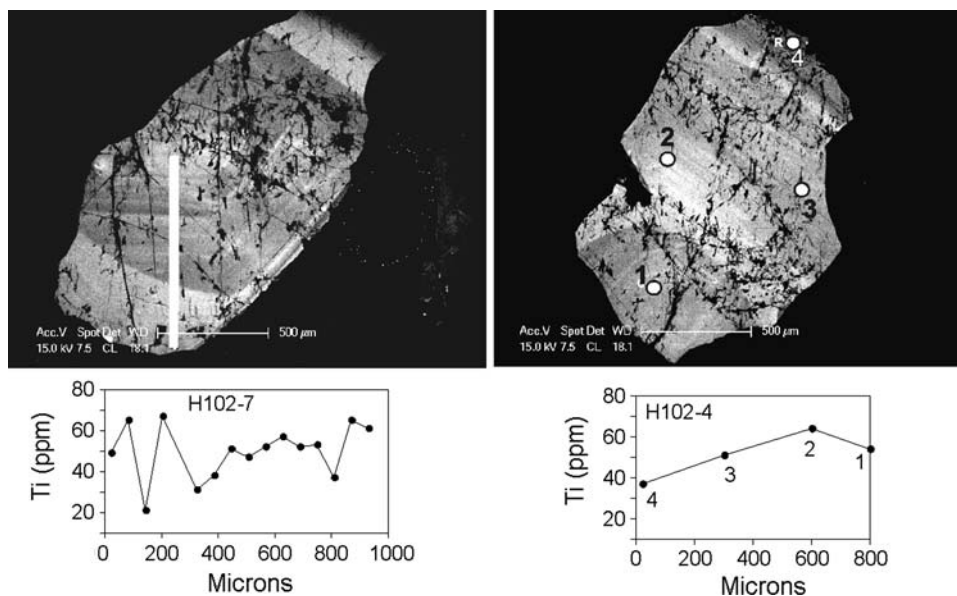
found within individual crystals from each of the three magma types (Fig. 5). Some of the greatest variations include 51–148 ppm Ti (731–861°C) in T3 crystal 907-4a (Fig. 5f); 46–128 ppm Ti (665–782°C) in crystal T2 952-1A (Fig. 5e); and 56–129 ppm (720–824°C) in T1 crystal 894-1. There are no overall trends in Ti distribution within crystals or within the 21.8 ka deposits (Fig. 7). The greatest compositional variation is found within individual crystals and is restricted to CL bright zones in mid-crystal bands (<150 μm in width) that equate to absolute temperature spikes of ~50–100°C amplitude. Core compositions of different crystals also vary greatly. For example, core variability in Ti (69 ± 28 ppm) of T1 crystals equates to temperature differences of up to ~140°C for commencement of growth.

With little mid-crystal variation in CL brightness in quartz from the 13.6 ka deposits (Fig. 5b), we focussed our analyses on core/rim contrasts. The crystal cores are relatively uniform (Ti = 65–96 ppm) and contrast with the brighter rims that have 85–111 ppm Ti (Fig. 7). Fifteen core–rim pairs were analysed; rims are between −1 to +41 ppm (average 17 ppm) higher than their cores. This Ti variation corresponds to temperature contrasts of up to 60°C. The highest quartz rim temperatures (770–790°C) are similar to Fe–Ti oxide estimates (772 ± 13°C) (Fig. 7).

Quartz from granitoid clasts in the 0.7 ka deposits have on average lower Ti contents (10–67 ppm) than the quartz analysed from pumices of other Tarawera episodes, and changes are more diffuse. Variations of 10–55 (H102–5A) and 21–67 ppm (H102–7) are found in broad zones within crystals (Fig. 6), and no overall within-crystal trends are evident in our limited data set, consistent with broader CL
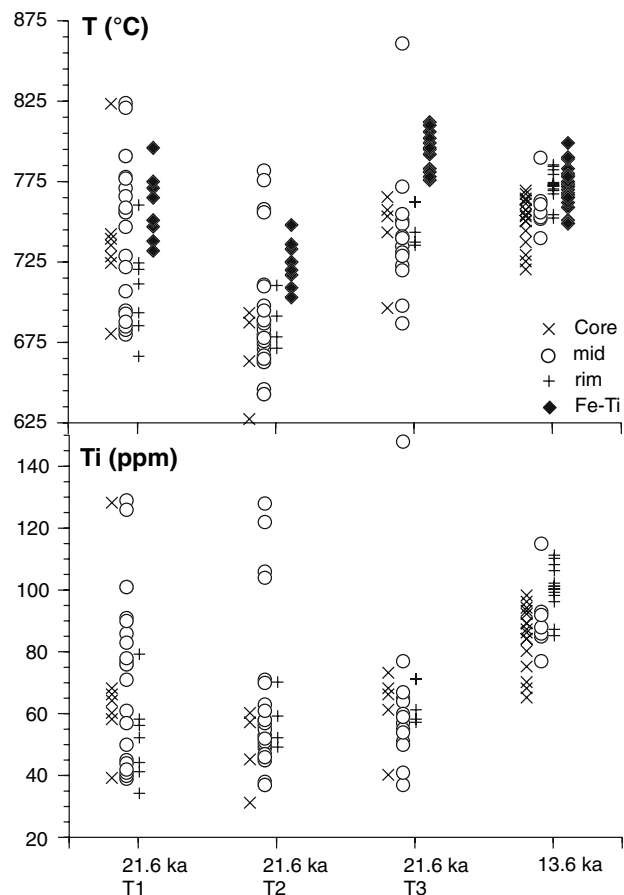
Fig. 7 Summary of Ti contents and temperature estimates for quartz from the 21.8 (T1-3 magmas) and 13.6 ka deposits classified according to analytical position in the crystal (core, mid, rim). Temperature based on Fe–Ti oxide equilibrium is shown for comparison

imaging. We did not estimate temperatures due to uncertainty in melt compositions for the granitoid clasts.

Discussion

Origin of the Tarawera rhyolite magmas

On the basis of trace element and isotope data, TVZ silicic magma genesis involved assimilation and fractional crystallisation (e.g., Graham et al. 1995). Elevated Sr isotope ratios argue against direct derivation from basaltic melts and require crustal assimilation. This is supported by the presence of ancient xenocrystic zircons (>90 Ma) found in some TVZ rhyolites (Charlier et al. 2005; Brown and Smith 2004) that are consistent with large scale melting of Mesozoic greywacke or later plutonic forerunners. Younger co-magmatic zircons in OVC rhyolites pre-date eruption ages by 50–100 kyears (Charlier et al. 2003), pointing to mid-crustal multi-cycle crystallisation and melting of silicic forerunners. Thus, we envisage a multi-level magmatic system beneath Tarawera, driven by deep mafic intrusion and involving mid-crustal multi-cycle crystallisation and melt extraction.

Mid-crustal crystal mush zone

Recent models for the production of relatively crystal-poor rhyolites highlight their origin as interstitial melts in crystal-mush zones where an open crystal framework allows the extraction of melts following tectonic and intrusive disturbances (e.g., Hildreth 2004; Bachmann and Berganz 2004; Eichelberger et al. 2006; Hildreth and Wilson 2007).

Several features are consistent with the existence of a long-lived crystal mush zone and crystal pile beneath Tarawera from which rhyolite melts have been episodically extracted. (1) The eruption of voluminous rhyolitic ignimbrites from OVC at 280 and ∼50 ka, along with other smaller eruptions, requires a long-lived magmatic system. The repeated extractions of crystal-poor melts (>300 km³ erupted) would have left a large volume of crystal residuum (e.g., Bachmann et al. 2007). (2) Negative Eu anomalies and high LREE/HREE ratios for Tarawera deposits (Table 1; Fig. 2e) and the preceding large volume ∼50 ka Rotoiti and Earthquake Flat pyroclastic deposits (Schmitz and Smith 2004; Molloy et al. 2008), indicate they are products of extensive plagioclase and hornblende fractionation, incurring large amounts of crystal residuum for each subsequent eruption. (3) Ejecta from Rotoiti and associated Earthquake Flat eruptions display textural and crystal zoning evidence that is consistent with the rejuvenation of near-crystalline plutons (Molloy et al. 2008). (4)

Pumices from these ∼50 ka eruptions contain zircons with ages spanning ∼300 kyears, demonstrating multi-stage heating and/or crystal inheritance from plutonic forerunners (Charlier et al. 2003). (5) Granitoid lithics in the ∼50 ka Rotoiti (Burt et al. 1998) and 0.7 ka Tarawera eruption ejecta, and microscopic crystal clots in 17.6 ka Tarawera pumice (Shane et al. 2007) point to the presence of associated crystalline bodies before these eruptions. (6) CL images of quartz in the 0.7 ka granitoid clasts show features similar to those described by Bernet and Bassett (2005) as micro-cracks in plutonic quartz, which they attribute to brittle deformation. This implies complete solidification of parts of the Tarawera magmatic system.

Several lines of evidence point to growth of OVC phenocrysts at ∼200 MPa, placing the crystal mush zone at <8 km depth, assuming an overburden density of ∼2,500 kg/m³. Evidence includes (1) rhyolite melt projection onto the Qtz–Ab–Or–water ternary diagram (Smith et al. 2005); (2) H_2O/CO_2 contents in quartz-hosted MIs (Shane et al. 2007, 2008); and (3) the presence of cummingtonite (Ewart et al. 1975) in many OVC magmas. The brittle–ductile boundary beneath TVZ is seismically located at ∼7 km and may influence the depth of magma ponding. Experimental work of Kavanagh et al. (2006) suggests that large lithospheric rigidity contrasts can arrest dykes, and promote sill formation.

A single, large melt cap on top of a crystal pile is not envisaged as the pre-eruption configuration of the Tarawera magmatic system. As detailed in our previous studies and here, spatially isolated melt pods are required for the co-eruption of different magma batches in some Tarawera episodes (Shane et al. 2007, 2008). Evidence for isolated melt pods includes (1) co-erupted crystal-rich and crystal-poor pumices, where crystal content does not relate to temperature; (2) the sequential and simultaneous emission of different magma types from spatially isolated vents up to 11 km apart; (3) individual pumice clasts containing bimodal glass compositions, crystal populations and T–fO_2 parameters demonstrating short-lived contact between mingled magmas; and (4) evidence for basaltic intrusion in all Tarawera episodes, but not in all the magma batches erupted during these episodes.

Multi-cycle crystallisation and re-melting

The various types of CL intensity patterns in quartz from the Tarawera deposits (Figs. 5, 6) are consistent with a multi-stage crystallisation history. Truncated CL patterns within crystals reflect resorption episodes, followed by crystal regrowth. Mid-crystal bright zones (∼150 μm wide) reflect significant magmatic fluctuations during the growth of the crystals, while bright rim mantles with sharp (<10 μm) internal boundaries reflect an abrupt

compositional and/or thermal change shortly before eruption. Some pumice clasts contain quartz crystals with either bright or dark cores indicating that crystals that had nucleated in different conditions had been juxtaposed in eruption.

Quartz CL intensity correlates directly with Al and Ti content. If no major changes occurred in the Ti activity of the melt within the individual magma batches, then the Ti content in the quartz directly reflects changes in temperature (e.g., Wark et al. 2007). The lack of variation in mineral assemblages within the individual Tarawera magma batches, and the ubiquitous presence of ilmenite, suggests that Ti activity in the melts was well buffered. If this assumption is correct, absolute temperature variations of ∼50–100°C amplitude are recorded within individual Tarawera quartz crystals, and between cores of crystals from the same pumices. Alternatively, some of the Ti variability may reflect inputs of new melts to the system that were sufficiently different in composition to overcome the buffering effects of the mineral assemblage. Both options require the addition of new magma into the system, which transfers heat and/or mixes with the rhyolite melt. Either way, open system processes are indicated.

The compositional contrasts between quartz-hosted MIs and accompanying matrix glasses in some Tarawera magma batches also demonstrate significant magmatic changes prior to eruption that cannot be explained by simple cooling in a closed system. Instead, they point to reactivation of a system that had been cooling. Matrix glasses in the 21.8 and 13.6 ka deposits that are enriched in Ba, Ti and Sr relative to their accompanying quartz-hosted MIs (Fig. 4) require the influx of a new melt. The recharging melt must have been silicic as Tarawera basalts have low Ba (<400 ppm, Nairn et al. 2004; Shane et al. 2008) and inmixing basalt would have lowered Ba values in the rhyolite matrix glass. Similar MI/matrix glass relationships have been reported in the Bishop Tuff and Lower Bandelier Tuff magmas (Hervig and Dunbar 1992; Roberge et al. 2005). For the Bishop Tuff magma, Wark et al. (2007) suggested that the new matrix melt originated by remelting of deeper parts of the crystal pile in response to basaltic intrusion, followed by upward percolation of this enriched melt into the overlying crystal mush. This concept also explains the regrowth of quartz at higher temperatures (to produce the bright CL rim mantles) as made possible by elevation of the quartz solidus induced by reduction of the activity of water. Such reduction can be driven by several processes, including the melting of anhydrous crystals, influx of CO_2 from the basalt, and transfer of water from the silicic melt into the basaltic melt (Wark et al. 2007; Wiebe et al. 2007).

A similar process of late-stage thermal and chemical recharge is indicated for the 13.6 ka Tarawera episode (Fig. 8). Many quartz crystals in the 13.6 ka deposits display Ti-enriched rims consistent with heating during crystal growth (Fig. 5b) to temperatures similar to those estimated from the (rapidly equilibrating) Fe–Ti oxides in the same pumices. Thus, the Sr and Ti-poor MIs in the 13.6 ka deposits were trapped at lower temperatures,
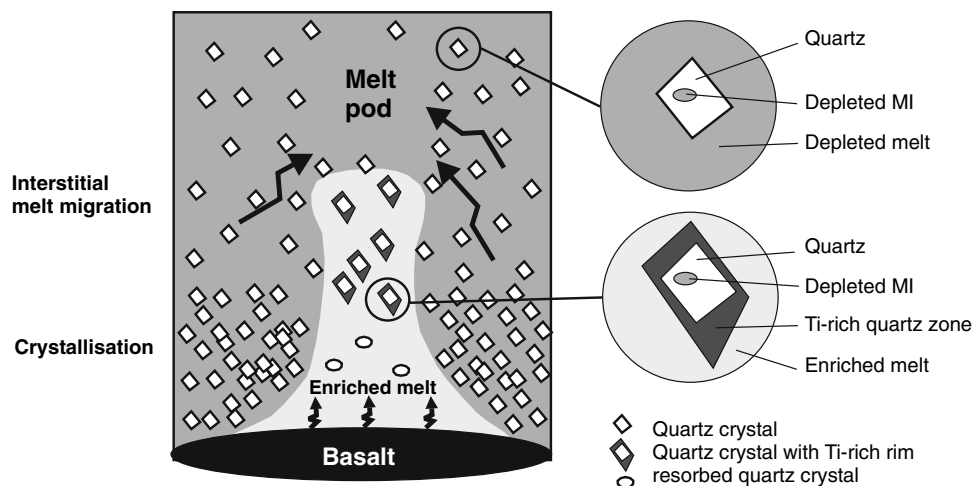
Fig. 8 Schematic diagram of silicic recharge and quartz Ti zoning processes (following Wark et al. 2007) in Tarawera magmas, exemplified by features in the 13.6 ka deposits. Early formed quartz crystals trapped evolved melt (depleted in Sr, Ba, Ti) as MIs during late stages of crystallisation. Basaltic intrusion re-melted the basal crystal pile to produce enriched (Sr, Ba, Ti) melt charged with CO_2 from basaltic degassing. The enriched melt plume migrated into the overlying crystal mush resulting in compositional changes in quartz crystals and mixing with interstitial melts in a process of convective self-mixing as described by Couch et al. (2001). Other eruption episodes such as the 21.8 ka event are envisaged as have undergone several such recharge events before eruption, producing mid-crystal zonation patterns in quartz

earlier in the crystallisation history (Fig. 8). The matrix glass trace element compositions vary on a cm-scale in the 13.6 ka pumice (Fig. 4b) and those of other Tarawera deposits, suggesting incomplete mixing of melt inputs. These non-equilibrated melts and crystals with different zoning histories occurring side-by-side in the same pumice clast, may reflect convective self-mixing processes where plumes from a re-activated boundary layer ascend into the overlying crystal mush (see Couch et al. 2001). Additional chaotic stirring may have occurred during melt extraction at eruption.

Although deposits of the 21.8 ka episode show similar MI/matrix glass relations to those of the 13.6 ka episode, their quartz CL patterns are more complex (Fig. 5c–f). Some Ti-rich rim mantles are evident, but many 21.8 ka quartz crystals display mid-crystal Ti-enriched zones indicating abrupt changes of the thermal and/or chemical environment during early to intermediate stages of crystal growth. Extensive crystal fragmentation in the 21.8 ka deposits prevents a full investigation of core–rim contrasts, but in general our data shows the highest Ti values occur in narrow mid-crystal zones.

Temperatures indicated by the Ti contents of 21.8 ka quartz rim zones are generally lower than Fe–Ti oxide estimates in the same magma batches (Fig. 7). We note that the two thermometers are independently derived and calibrated, and there could be unrecognised changes in Ti activity during the history of the melt. However, diffusion rates could explain differences in the recorded signals. Abrupt changes in Ti across quartz profiles would gradually become dampened by diffusion at elevated temperatures. In 21.8 ka quartz, Ti content varies by up to 90 ppm over distances of <30 μm (Fig. 5f). These gradients are comparable to those found in Bishop Tuff and Vinalhaven granite quartz where it has been estimated that such variations would be eliminated by diffusion over periods $>10^2$–10^3 years at 700–800°C (see Wark et al. 2007; Wiebe et al. 2007). In contrast, Fe–Ti oxides can re-equilibrate in days to months (Devine et al. 2003). Thus, Fe–Ti oxides are more likely to record the final melt temperature before eruption (possibly a triggering thermal pulse), while the quartz crystals record earlier and longer period fluctuations in the magmatic system. Shane et al. (2008) highlight basaltic intrusion as the final eruption trigger for the 21.8 ka episode. Although three physiochemically discrete magmas can be distinguished in the 21.8 ka deposits, each displays similar quartz zoning and MI/matrix glass compositional contrasts indicating that they all experienced multiple thermal and chemical recharges before the eruption. This indicates that heat, volatiles and liquids pervasively permeated the upper crystal mush zone that contained the isolated magma "pods".

MI/matrix glass compositional contrasts in the 0.7 ka juvenile ejecta differ significantly from those of the 21.8 and 13.6 ka episodes, and demonstrate the variable magmatic history of Tarawera over the last 22 kyears. In the 0.7 ka deposits, MIs display a range in composition that is mostly less evolved (higher Sr, Ti) than the accompanying matrix glass (Fig. 4c, g). Although the MIs follow a general trend expected from crystallisation of plagioclase (Fig. 4g), evidence does not indicate that Rayleigh-style fractional crystallisation controlled the entire melt composition. Similar to other Tarawera deposits, multiple glass analyses show that trace element compositions are not uniform over a cm-scale between or within pumice clasts in 0.7 ka deposits (Fig. 4a). This would be best explained by new melt input(s) and various degrees of partial homogenisation. Thus, the quartz crystals may have been variously inherited from different melts or crystallisation stages.

Cathodoluminescence images of 0.7 ka quartz generally show bright cores with gradual change to darker rims consistent with cooling during growth. Although periods of resorption are evident, there are no bright rims that would reflect late-stage thermal signals. This is despite strong evidence for basaltic intrusion having triggered the eruption from repeated intrusions (Leonard et al. 2002; Nairn et al. 2004). Amphibole growth in the basaltic intruder has also been argued as an indication of water absorption (Nairn et al. 2004) and hence a reduction in water activity in the rhyolite would be expected. Thus, the lack of late-stage quartz overgrowths suggests insufficient time following the thermal pulse for crystal growth to record the final thermal signal.

Conclusions

The eruption history at Tarawera provides insights into the evolution of a silicic magmatic system on a millennial timescale. Heterogeneity between pumice clasts in most Tarawera deposits demonstrates that separate rhyolite magma pods, with distinct physiochemical properties, existed contemporaneously and experienced different crystallisation histories, within an upper-crustal crystal mush zone. Vent locations and eruption sequences show that some contemporaneous magma bodies were laterally separated on a km-scale. Insufficient time or intervening spatial barriers prevented mixing and re-equilibration of these magma pods. Mingling between co-erupted magmas was restricted to short-lived contact in the conduit as demonstrated by disequilibrium Fe–Ti oxides and mingled glasses in some pumices and lavas. The magma pods were transient, with melt formation and depletion on a 10^3-year scale.

The magma batches are defined from properties at a large spatial scale (whole pumice). However, they are more heterogeneous on cm- and mm-scales. Matrix glasses within individual pumice clasts show wide variations in trace element composition pointing to open system recharge and indicating incomplete mixing of rhyolite melts. CL zoning and Ti contents in quartz in some of the magma batches demonstrate a multi-stage crystallisation history involving periods of crystal resorption alternating with regrowth. Bright and dark CL cored crystals occur side-by-side in some pumice clasts indicating nucleation in differing conditions. CL brightness correlates to Ti content, which is influenced by temperature. Thus, abrupt mid-crystal or rim mantle spikes in Ti (up to 90 ppm amplitude) in many crystals reflect rapid changes in melt chemistry and/or temperature (~ 50–$100°C$ amplitude). Such open system behaviour is also supported by quartz-hosted MI chemistry that differs from accompanying matrix glass in many of the magmas. In some magmas, rhyolitic recharge melts enriched in compatible trace elements percolated into the overlying crystal mush to envelop quartz crystals left from earlier crystallisation events. These recharge events probably resulted from deep basaltic intrusion and re-melting of the crystal pile. Contemporaneous magma pods experienced similar rejuvenating or recharge events indicating widespread percolation of new melts through the magmatic system. However, these recharge events were of insufficient volume or of too limited duration, to result in complete re-equilibration or masking of original physico-chemical properties of the magma pods that were inherited from different cooling histories and/or heterogeneities in the crystal mush.

Subordinate basaltic components in the ejecta of each of the eruption episodes indicate that basaltic intrusion was the final trigger for the Tarawera rhyolite eruptions. While Fe–Ti oxides reflect quench temperatures, the quartz crystals record longer period (10^2–10^3 years) temperature fluctuations, and along with the MI evidence, show that repeated basaltic intrusions produced the erupted rhyolite magmas by recycling of the crystal mush zone.

The recording of these thermal and chemical fluxes in magmas over short periods ($<10^3$ year) reflects the thin and actively rifting crust in the TVZ, which has promoted rapid magma production and eruption, rather than stagnation, accumulation and homogenisation (or stratification) at depth. In a less active tectonic setting, amalgamation of the magma batches may have obscured the 10^2–10^3 year-period fluctuations. The frequent eruption sampling at Tarawera has provided evidence that supports the concept of incremental growth of silicic magma systems that are heterogeneous, transient and never completely liquid.

References

Bachmann O, Bergantz GW (2004) On the origin of crystal-poor rhyolites: extracted from batholithic crystal mushes. J Petrol 45:1565–1582

Bachmann O, Dungan MA, Lipman PW (2002) The Fish Canyon magma body, San Juan volcanic field, Colorado: rejuvenation and eruption of an upper-crustal batholith. J Petrol 43:1469–1503

Bachmann O, Miller CF, de Silva SL (2007) The volcanic–plutonic connection as a stage for understanding crustal magmatism. J Volcanol Geotherm Res 167:1–23

Bannister S, Bryan CJ, Bibby HM (2004) Shear wave velocity variation across the Taupo Volcanic Zone, New Zealand, from receiver function inversion. Geophys J Int 159:291–310

Bernet M, Bassett K (2005) Provenance analysis by single-quartz-grain SEM-CL/optical microscopy. J Sediment Res 75:492–500

Brown SJA, Smith RT (2004) Crystallisation history and crustal inheritance in a large silicic magma system: 206Pb/238U ion probe dating of zircons from the 1.2 Ma Ongatiti ignimbrite, Taupo Volcanic Zone. J Volcanol Geotherm Res 135:247–257

Brown SJA, Burt RM, Cole JW, Krippner SJP, Price RC, Cartwright I (1998) Plutonic lithics in ignimbrites of Taupo Volcanic Zone, New Zealand; sources and conditions of crystallisation. Chem Geol 148:21–41

Burt RM, Brown SJA, Cole JW, Shelley D, Waight TE (1998) Glass-bearing plutonic fragments from ignimbrites of the Okataina caldera complex, Taupo Volcanic Zone, New Zealand: remnants of a partially molten intrusion associated with preceding eruptions. J Volcanol Geotherm Res 84:209–237

Bryan CJ, Sherburn S, Bibby HM, Bannister S, Hurst AW (1999) Shallow seismicity of the central Taupo Volcanic Zone, New Zealand: its distribution and nature. NZ J Geol Geophys 42:533–542

Charlier BLA, Peate DW, Wilson CJN, Lowenstern JB, Storey M, Brown SJA (2003) Crystallisation ages in coeval silicic magma bodies: ^{238}U–^{230}Th disequilibrium evidence from the Rotoiti and Earthquake Flat eruption deposits, Taupo Volcanic Zone, New Zealand. Earth Planet Sci Lett 206:441–457

Charlier BLA, Wilson CJN, Lowenstern JB, Blake S, van Calsteren PW, Davidson JP (2005) Magma generation at a hyperactive silicic volcano (Taupo, New Zealand) revealed by U–Th and U–Pb systematics in zircons. J Petrol 46:3–36

Couch S, Sparks RSJ, Carroll MR (2001) Mineral disequilibrium in lava explained by convective self-mixing in open magma chambers. Nature 411:1037–1039

Darragh M, Cole J, Nairn I, Shane P (2006) Pyroclastic stratigraphy and eruption dynamics of the 21.9 ka Okareka and 17.6 ka Rerewhakaaitu eruption episodes from Tarawera Volcano, Okataina Volcanic Centre, New Zealand. NZ J Geol Geophys 49:309–328

Devine JD, Rutherford MJ, Norton GE, Young SR (2003) Magma storage region processes inferred from geochemistry of Fe–Ti oxides in andesitic magma, Soufriere Hills Volcano, Montserrat, W.I. J Petrol 44:1375–1400

D'Lemos RS, Kearsley AT, Pembroke JW, Watt GR, Wright P (1997) Complex quartz growth histories in granite revealed by scanning cathodoluminescence techniques. Geol Mag 134:549–552

Eichelberger JC, Izbekov PE, Browne BL (2006) Bulk chemical trends at arc volcanoes are not liquid lines of decent. Lithos 87:135–154

Ewart A, Hildreth W, Carmichael ISE (1975) Quaternary acid magma in New Zealand. Contrib Mineral Petrol 51:1–27

Glazner AF, Bartley JM, Coleman DS, Gray W, Taylor RZ (2004) Are plutons assembled over millions of years by amalgamation from small magma chambers. GSA Today 14:4–10

Graham IJ, Cole JW, Briggs RM, Gamble JA, Smith IEM (1995) Petrology and petrogenesis of volcanic rocks from Taupo Volcanic Zone: a review. J Volcanol Geotherm Res 68:59–87

Harrison AJ, White RS (2004) Crustal structure of the Taupo Volcanic Zone, New Zealand: stretching and igneous intrusion. Geophys Res Lett 31:L13613. doi:10.1029/2004GL019885

Hayden LA, Watson EB, Wark DA (2005) Rutile saturation and TiO_2 diffusion in hydrous siliceous melts. EOS: Fall meeting supplement abstracts 86, MR13A-0076

Heise W, Bibby HM, Caldwell TG, Bannister SC, Ogawa Y, Takakura S, Uchida T (2007) Melt distribution beneath a young continental rift: the Taupo Volcanic Zone, New Zealand. Geophys Res Lett 34:L14313

Hervig RL, Dunbar NW (1992) Causes of chemical zoning in the Bishop (California) and Bandelier (New Mexico) magma chambers. Earth Planet Sci Lett 111:97–108

Hildreth W (2004) Volcanological perspectives on Long Valley, Mammoth Mountain, and Mono Craters: several contiguous but discrete systems. J Volcanol Geotherm Res 136:169–198

Hildreth W, Wilson CJN (2007) Compositional zoning of the Bishop Tuff. J Petrol 48:951–999

Kavanagh JL, Menand T, Sparks RSJ (2006) An experimental investigation of sill formation and propagation in layered elastic media. Earth Planet Sci Lett 245:799–813

Leonard GS, Cole JW, Nairn IA, Self S (2002) Basalt triggering of the AD1305 Kaharoa rhyolite eruption episode, Tarawera volcanic complex, New Zealand. J Volcanol Geotherm Res 115:461–486

Lipman PW (2007) Incremental assembly and prolonged consolidation of Cordilleran magma chambers: evidence from the southern Rocky Mountain volcanic field. Geosphere 3:42–70

Molloy C, Shane P, Nairn I (2008) Pre-eruption thermal rejuvenation and stirring of a partly crystalline rhyolite pluton revealed by the Earthquake Flat Pyroclastics deposits, New Zealand. J Geol Soc Lond 165:435–447

Nairn IA (2002) Geology of the Okataina Volcanic Centre, scale 1:50 000. Institute of Geological and Nuclear Sciences geological map 25. Institute of Geological and Nuclear Sciences, Lower Hutt, New Zealand, p 156 + 1 sheet

Nairn IA, Cole JW (1981) Basalt dikes in the 1886 AD Tarawera rift. N Z J Geol Geophys 24:585–592

Nairn IA, Self S, Cole JW, Leonard GS, Scutter C (2001) Distribution stratigraphy and history of proximal deposits from the c. AD 1305 Kaharoa eruptive episode at Tarawera volcano, New Zealand. NZ. J Geol Geophys 44:467–484

Nairn IA, Shane P, Cole JW, Leonard GJ, Self S, Pearson N (2004) Rhyolite magma processes of the ∼AD1315 Kaharoa eruptive episode, Tarawera volcano, New Zealand. J Volcanol Geotherm Res 131:265–294

Nairn IA, Hedenquist JW, Villamor P, Berryman KR, Shane PA (2005) The ∼AD1310 Tarawera and Waiotapu eruptions, New Zealand: contemporaneous rhyolite and hydrothermal eruptions driven by an arrested basalt dike system? Bull Volcanol 67:186–193

Peppard BT, Steele IM, Davis AM, Wallace PJ, Anderson AT (2001) Zoned quartz phenocrysts from the rhyolitic Bishop Tuff. Am Mineral 86:1034–1052

Roberge J, Wallace PJ, Kent AA (2005) The origin of quartz phenocrysts in the Bishop Tuff rhyolitic magma based on trace elements in melt inclusions and pumice matrix glass. EOS 86: Fall meeting supplement, abstract V13B-0524

Ryerson FJ, Watson EB (1987) Rutile saturation in magmas: implications for Ti–Nb–Ta depletion in island arc basalts. Earth Planet Sci Lett 86:225–239

Schmitz MD, Smith IEM (2004) The petrology of the Rotoiti eruption sequence, Taupo Volcanic Zone: an example of fractionation and mixing in a rhyolitic system. J Petrol 45:2045–2066

Shane P, Martin SB, Smith VC, Beggs KF, Darragh MB, Cole JW, Nairn IA (2007) Multiple rhyolite magmas and basalt injection in the 17.7 ka Rerewhakaaitu eruption episode from Tarawera volcanic complex, New Zealand. J Volcanol Geotherm Res 164:1–26

Shane P, Nairn IA, Smith VC, Darragh M, Beggs KF, Cole J (2008) Multi-stage mafic and silicic recharge of multiple rhyolite magmas during the 22.6 ka Okareka Eruption Episode, New Zealand. Lithos (in press)

Skirius CM, Peterson JW, Anderson AT (1990) Homogenizing rhyolitic glass inclusions from the Bishop Tuff. Am Mineral 75:1381–1398

Smith VC, Shane P, Nairn IA (2005) Trends in rhyolite geochemistry, mineralogy, and magma storage during the last 50 kyear at Okataina and Taupo volcanic centres, Taupo Volcanic Zone, New Zealand. J Volcanol Geotherm Res 148:372–406

Speed J, Shane P, Nairn I (2002) Volcanic stratigraphy and phase chemistry of the 11 900 year BP Waiohau eruptive episode, Tarawera Volcanic Complex, New Zealand. NZ J Geol Geophys 45:395–410

Stern TA, Stratford WR, Salmon ML (2006) Subduction evolution and mantle dynamics at a continental margin: central North Island, New Zealand. Rev Geophys 44:RG4002. doi:10.1029/2005RG000171

Stratford WR, Stern TA (2004) Strong seismic reflections and melts in the mantle of a continental back-arc basin. Geophys Res Lett 31:L06622. doi:10.1029/2003GL019232

Wark DA, Watson EB (2006) The TitaniQ: a titanium-in-quartz geothermometer. Contrib Mineral Petrol 152:743–754

Wark DA, Hildreth W, Spear FS, Cherniak DJ, Watson EB (2007) Pre-eruption recharge of the Bishop magma system. Geology 35:235–238

Wiebe RA, Manon MR, Hawkins DP, McDonough WF (2004) Late-stage mafic injection and thermal rejuvenation of the Vinalhaven Granite, coastal Maine. J Petrol 45:2133–2153

Wiebe RA, Wark DA, Hawkins DP (2007) Insights from quartz cathodoluminescence zoning into crystallization of the Vinalhaven granite, coastal Maine. Contrib Mineral Petrol 154:439–453